Received 8 July 2021; revised 1 September 2021; accepted 16 September 2021. Date of publication 23 September 2021;
date of current version 5 October 2021. The review of this article was arranged by Editor A. Nathan.

Digital Object Identifier 10.1109/JEDS.2021.3115027

Impact of Die Carrier on Reliability of Power LEDs

SHUSMITHA KYATAM, LUIS N. ALVES (Member, IEEE), STANISLAV MASLOVSKI, AND JOANA C. MENDES (Member, IEEE)

Instituto de Telecomunicações e Departamento de Electrónica, Telecomunicações e Informática, University of Aveiro, 3810-193 Aveiro, Portugal

CORRESPONDING AUTHOR: J. C. MENDES (e-mail: joanacatarina.mendes@ua.pt)

This work was supported by FCT/MCTES through National Funds and when applicable co-funded by EU Funds under Project UIDB/50008/2020-UIDP/50008/2020.

ABSTRACT High power light emitting diodes (LEDs) suffer from heating effects that have a detrimental impact on the devices characteristics. The use of LED carriers with high thermal conductivity promotes extraction of heat away from the LED junction. Different materials can be used for this purpose, such as alumina, aluminium nitride, and silicon. Diamond has also been gaining momentum for demanding heat management applications. In order to evaluate the impact of the carrier material on the reliability of the devices, the junction temperature of Cree white XLamp XB-D LEDs was obtained with Ansys for various carriers and different LED current levels. The impact of the junction temperature on the LED's lifetime, emission intensity, footprint, and wavelength stability was then evaluated for each carrier based on the datasheet of the devices. The results provide additional knowledge regarding the impact of the carrier on the performance of the LED.

INDEX TERMS Light-emitting diodes, reliability, diamond, packaging.

I. INTRODUCTION

High power light emitting diodes (LEDs) have revolutionized lighting applications. LEDs are compact devices with high lighting capability and spend only a fraction of the energy of filament bulbs. Nevertheless, these devices suffer from self-heating issues. Non-radiative recombination in the LED active region generates most of the heat at low current levels and, at high current levels, the parasitic resistances of the contacts and cladding layers provide an additional source of heat. Considering all these contributions, the efficiency of the LEDs stays below 30%. As a rule of thumb, LED lumen output typically decreases 0.3-0.5% for each 1°C increase in the junction temperature (T_J) [1]. Similarly to what happens with other semiconductor devices, the increase of T_J has a negative impact on both life time and reliability of the LEDs. Finally, the energy gap of the semiconductor depends on the temperature [2]; as a consequence, the wavelength of the emitted light increases with T_J. While the stability of the wavelength alone is not relevant for lighting applications, the associated change in the chromaticity of the LEDs may induce changes in the perception of object colors.

In order to facilitate the extraction of light from the device, the LED die is typically encapsulated inside a dome-shaped material with a large refractive index; however, dome materials are typically poor heat conductors, and this hinders the removal of heat by convection. To promote the efficient removal of the heat from the die, researchers and manufacturers have proposed different solutions that minimize the thermal resistance of the package. As an example, the integration of a copper (Cu) heat spreader increases the power efficiency by 3% when compared to a conventional package [3]. The use of flip-chip architecture provides an efficient means to decrease the thermal resistance of the package, especially if combined with carriers with large thermal conductivity (κ). Among the typically used materials one can find alumina (Al_2O_3) [4], silicon (Si) [5], or aluminium nitride (AlN) [6], [7]. Chun *et al.* [8] went one step beyond and integrated the LED die with a Si thermoelectric cooler (TEC) MEMS using flip-chip. The impact of the solder pads, solder bumps, and die attach [1], [4], [5], [9], and underfills [5], [7] has also been evaluated by different researchers.

The carrier has an obvious impact on the thermal resistance of a LED package. In the case of surface mount devices (SMD), for instance, if one neglects the die attach and solder layers, the heat generated in the LED die active layers has

This work is licensed under a Creative Commons Attribution 4.0 License. For more information, see https://creativecommons.org/licenses/by/4.0/

to travel through the die substrate and carrier (when die and carrier are assembled via wire bonding) or through the carrier alone (in case of flip-chip architecture) before it reaches the back side of the LED package. Thus, for a given package layout, T_J depends on the carrier and materials with high κ are desired.

Carbon-based materials, such as diamond, highly oriented pyrolytic graphite (HOPG), and graphene, are obvious candidates. Due to its structure, HOPG is an anysotropic thermal conductor ($\kappa_{\text{in-plane}} \simeq 2000$ W/(m·K) while $\kappa_{\text{out-plane}}$ is two orders of magnitude lower [10]). If assembled with the die adequately, HOPG carriers could facilitate the transfer of the heat generated in the die towards the back side of the carrier. However, HOPG is also electrically conductive, and this creates some problems with respect to the insulation of the terminals of the p-n junction. Graphene features an even higher in-plane κ (2000-4000 W/(m·K)), however graphene sheets are also electrically conductive. In addition, since graphene is a 2D material (monolayer thickness $\simeq$3.35 Å [11]), one can't take advantage of the in-plane κ and promote the transfer of heat to the back of the device. Despite these limitations, one can find recent reports describing the use of graphene for thermal management applications [12].

Diamond is an isotropic material that features simultaneously a high thermal conductivity (2200 W/(m·K), increasing to 3300 W/(m·K) in the case of isotopically pure material) while being an electric insulator, with a breakdown field as high as 2×10^7 V/cm [13]. Given these extreme properties, diamond has been used for the thermal management of electronic components at various levels. Its use as a heat sink material was proposed back in 1967, when Swan reported that Si avalanche diodes mounted on a single crystal diamond carrier achieved a continuous power density more than twice the one obtained with copper heat sinks [14]. Other reports on the use of diamond as a heat sink followed, a complete list can be found in [15]. Free standing diamond has also been used as a sub-mount for lasers [16], [17] as well as a circuit board integrated with water-cooling channels [18]. Gallium nitride (GaN) high electron mobility transistors (HEMTs) also benefit from the integration with diamond films [19]–[23].

Diamond has also been used to improve the thermal management of power LEDs at different levels. Horng *et al.* [3] mounted the LED die on a diamond-coated copper heat sink and obtained an 11°C reduction in T_J in comparison to mounting the LED on a conventional MCPCB. Chen *et al.* [24] reported a 20°C reduction in T_J at 1 A when the LED chips were bonded on Si substrates coated with 20 μm of diamond. Fan *et al.* [25] replaced the Cu heat sink of white power LEDs with a diamond/Cu composite material and obtained a reduction on the weight of the internal heat sink by more than 35% and simultaneously a decrease in the thermal resistance and T_J by as much as 10.5% and 33.3%, respectively. Diamond films have also been integrated directly with the LED die in grooves etched on the upper ITO layer of LEDs [26].

Despite the promising results of these different to the authors' best knowledge of a diamond plate as the carrier of power LED dies has not been reported yet. This paper aims at estimating the expected benefits of such an approach. To this end, the temperature profiles of Cree white XLamp XB-D power LEDs were obtained with Ansys. Different carriers were considered in the simulations: AlN (the actual carrier, as described by the manufacturer), Al_2O_3, Si, and diamond. The results were used to estimate the acceleration factor (AF) and the change in the relative luminous flux (RLF) when the AlN carrier is replaced with a material with different thermal properties. The dependency of the wavelength on the current level of monochromatic LEDs mounted on different carriers was also estimated.

II. SIMULATIONS AND MODELING

A. LED STRUCTURE

The thermal analysis was performed for the package of Cree white XLamp XB-D LEDs. These devices have a small footprint (2.45×2.45 mm^2), a maximum current rating of 1 A and are available in different colors (white, blue, green, amber, and red). The cross-section schematic view of the LEDs can be seen in Fig. 1(a) [27], [28]. According to information provided by the manufacturer, the LED die (in blue) is attached to an AlN carrier (in grey) and the junction terminals are electrically connected to the Cu electrodes (red shapes) via bond wires. The die is composed of a silicon carbide (SiC) substrate [29] with the GaN active layers [30] on top. Fig. 1(b) shows the top view of the LED without the epoxy dome, with the electrode pads (red shapes) and via holes (green circular shapes) clearly visible. Fig. 1(c) shows the bottom view of the LED; the electrode in the middle corresponds to the thermal pad. The dimensions and properties of each part are listed in Table 1.

To evaluate the impact of the carrier on the reliability of the LED, the simulations were performed for different materials. In addition to Al_2O_3, AlN, and Si (materials typically used for this purpose), diamond carriers were also considered. Al_2O_3 and AlN are available in ceramic and crystalline forms, with significantly different values of κ. In order to account for this variation, the simulations were performed with the minimum and maximum values of κ found in the literature for the ceramic and crystalline forms [31]–[37]. Diamond is also available as a single crystal (SCD) or as a polycrystalline (PCD) material [38], [39]; both types were considered in the simulations. The κ of the different materials is listed in Table 1.

B. NUMERICAL SIMULATIONS

The simulations were performed using Ansys multiphysics software (package Mechanical). The structure of the LED was created using the information from manufacturer as in Table 1; the die-attach layer was neglected and the thermal contact between the GaN+SiC die and the carrier was considered to be perfect.

TABLE 1. Dimensions and thermal conductivity of LED parts.

Part	Material	Thickness (μm)	Area (mm^2)	Thermal Conductivity (W/(m·K))
Carrier	ceramic Al_2O_3	540	2.45×2.45	27 [31] / 35 [32]
	single crystal Al_2O_3			42 [33]
	ceramic AlN			60 [34] / 193 [35]
	single crystal AlN			285 [36]
	single crystal Si			148 [37]
	polycrystalline diamond			1800 [38]
	single crystal diamond			2200 [39]
Led die	GaN	5	1.06×1.06	230 [40]
	SiC	140	1.06×1.06	430 [41]
Top electrodes	Cu	110	2.29×0.36	400 [42]
Bottom electrodes	Cu	110	2.29×0.33	400 [42]
Bottom thermal pad	Cu	110	2.29×0.92	400 [42]
Vias holes	Solder	540	4.07×10^{-3}	48 [42]
Epoxy	Silicone	220 [1] / 1090 [2]	4 mm^3 [3]	0.3 [43]

[1] rectangle thickness; [2] dome radius; [3] volume.

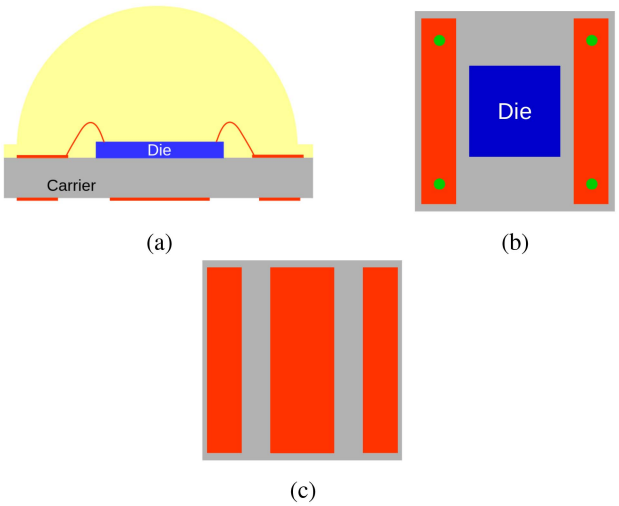

FIGURE 1. (a) LED cross-section view. (b) LED top view without epoxy dome. (c) LED bottom view. Drawings not to scale.

After being generated, the mesh was validated using Ansys built-in validation tools. An element quality measure lower than 5×10^{-6} was used; this metric is based on the ratio of the volume to the sum of the squares of the edge lengths for the three-dimensional (3D) mesh elements, which, according to the Ansys Meshing User's guide, has proven to be effective for thermal problems.

The thermal power P_{Th}, calculated as 75% of the electric power P_{El} [44], was considered to be generated inside the 5-μm-thick GaN layer and the temperature of the three bottom electrodes was kept at 40°C. This assumption corresponds to mounting the LED directly on a TEC; even though this may not correspond to a realistic scenario, it "forces" the transfer of heat across the different components of the LED and allows for a more direct evaluation of the impact of the κ of the carrier on T_J. The heat generated within the active layers of the die was also considered to be dissipated by convection from the epoxy and from the lateral sides of the carrier; the convective film coefficient had the default value assumed by Ansys (5 W/(m^2·K)).

The simulations were performed for current levels I between 100 and 800 mA with a step of 100 mA and for 350 mA (nominal current value according to the manufacturer). The electric power P_{El} was calculated as the product of the diode forward current I and the forward voltage V, which, in turn, were determined from the LTSpice model for the Xamp XB-D LED [45].

III. RESULTS AND DISCUSSION

A. IMPACT OF THE CARRIER ON THE JUNCTION TEMPERATURE

The simulated values of T_J are plotted as a function of I for each carrier in Fig. 2(a) with solid symbols. The respective trend lines are also represented as solid lines. As expected, T_J decreases with increase of the κ of the carrier. It is clear that not only the type of material (Al_2O_3, AlN, Si, or diamond) but also the quality (single crystal vs ceramic) have a large impact on T_J. As an example, if the lowest quality Al_2O_3 is used as the carrier, T_J increases by 6°C with respect to T_J obtained with the single crystal form. A similar situation happens with AlN; T_J increases by $\simeq$6.6°C with the lowest quality material. Regarding Si, the simulations were performed considering only the crystalline material with a κ = 148 W/(m·K). Ceramic AlN can have a higher (193 W/(m·K)) or lower (60 W/(m·K)) κ; as a consequence the T_J obtained with Si may be higher or lower than then the one obtained with AlN, depending on the quality of the latter. Replacing crystalline AlN with PCD (κ = 1800 W/(m·K)) reduces T_J by $\simeq$1.7°C; the use of SCD only brings a further $\simeq$0.1°C benefit.

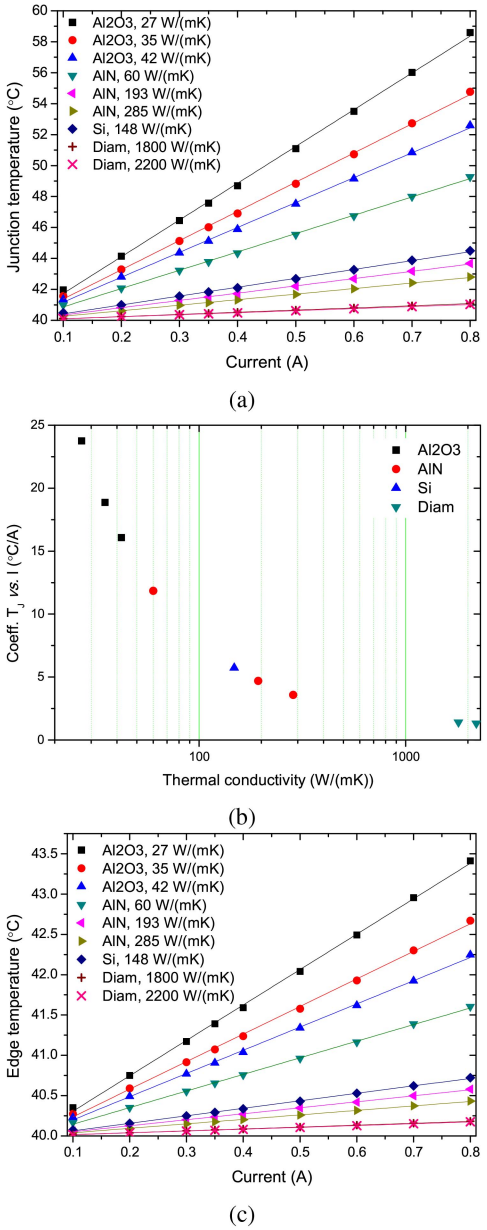

FIGURE 2. **(a) T_J and respective trend lines as a function of I. (b) Slope of $T_J(I)$ curves as a function of the κ of the carrier. (c) Edge temperature as a function of I.**

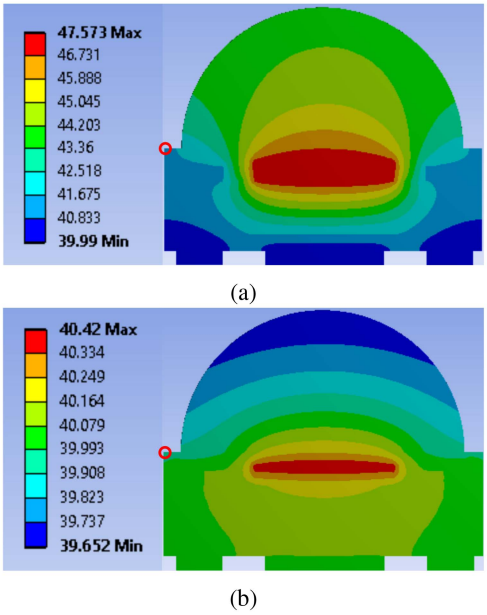

FIGURE 3. **Cross-section temperature maps at 350 mA with (a) Al_2O_3 (27 W/(m·K)) and (b) diamond (2200 W/(m·K)). The red circles show the position where the edge temperature was measured.**

The temperature maps obtained with the two extreme materials for 350 or 800 mA are shown in Figs. 3 and 4, respectively. Figs. 3(a) and 4(a) were obtained with Al_2O_3, 27 W/(m·K) and Figs. 3(b) and 4(b) with diamond, 2200 W/(m·K). The difference in T_J is notorious: for nominal current (350 mA), T_J reaches 47.6 and 40.4°C with Al_2O_3 and SCD, respectively ($\simeq$7.2°C difference). Similarly, if the current rises to 800 mA, T_J increases to 58.6 and 41.0°C ($\simeq$17.6°C difference) for the same materials. Independently of the current level, the SCD carrier behaves nearly as a thermal short circuit, keeping T_J close to the temperature imposed by the TEC.

The impact of the carrier on T_J can also be evaluated by calculating the slope of the $T_J(I)$ curves, which is depicted in Fig. 2(b) as a function of the κ of the carrier. A lower slope value indicates a smaller dependency of T_J on the level of current. The slope varies considerably with the quality of Al_2O_3 (between $\simeq$16 and $\simeq$24°C/A) and AlN (between $\simeq$3.6 and $\simeq$12°C/A) and reaches its minimum value with the diamond carriers. No significant difference is observed between SCD and PCD materials ($\simeq$1.4°C/A).

It should be mentioned that the apparently linear dependence of T_J with I is a consequence of the assumptions made in the implementation of the simulations. The first assumption is the validity of the LTSpice model used to calculate the voltage drop across the LED for the different levels of I. This model is valid for $T_J = 25$°C, whereas in our case the values of T_J are higher. In addition, for a given I, T_J varies with the carrier. Since the LED voltage also depends on T_J, the use of this simple LTSpice model introduces an error in the determination of the electric power P_{El} for a given I. Nevertheless, for this particular model, an increase of 10 times (900%) in the current is accompanied by a change in the LED voltage smaller than 20%, so this is not considered to be the main source of error. The most relevant assumption is the consideration that P_{Th} is 75% of P_{El} for all levels of I. The 25% efficiency is valid for nominal operating conditions [44]. As the current increases, the efficiency of the LED decreases, so the dissipated power (and correspondingly T_J) increases. However, and despite this assumption contributes with an error that may not be negligible, taking into account the temperature-dependent efficiency would increase the difference in the thermal performance of the carriers even more. By assuming a constant efficiency, we are indirectly

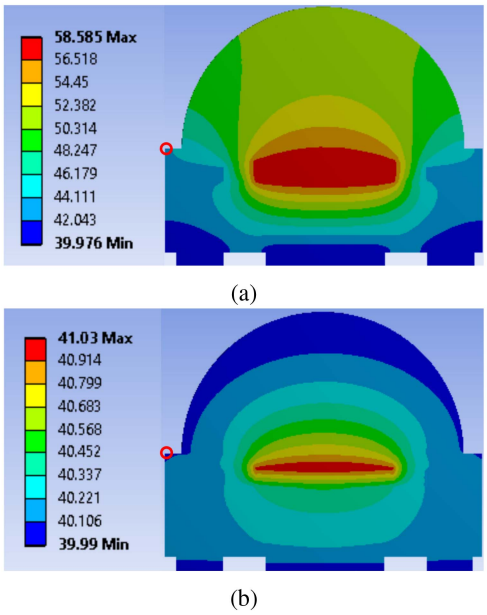

FIGURE 4. Cross-section temperature maps at 800 mA with (a) Al_2O_3 (27 W/(m·K) and (b) diamond (2200 W/(m·K)). The red circles show the position where the edge temperature was measured.

limiting the difference in the performance of the different carriers. The impact of considering a temperature-dependent efficiency will be a part of our future work.

The carrier also influences the thermal footprint of the LED die. This can be seen in Fig. 2(c), that shows the temperature at a position close to the edge of the carrier (marked with a red circle in Figs. 3 and 4) for the different current levels. With Al_2O_3 (27 W/(m·K)), this temperature is as high as 41.4 and 43.4°C for 350 and 800 mA, respectively, whereas the temperature with diamond (2200 W/(m·K)) at the same location stays at ≃40.1 and ≃40.2°C for the same current levels, respectively. The values of temperature at the edge of the carrier obtained with the other materials are between these extreme values. The impact of the carrier on the device footprint becomes more apparent if one looks at the cross-section temperature maps obtained with a current level of 350 and 800 mA for the two extreme materials (Figs. 3 and 4). With the diamond carrier, the temperature at the immediate vicinity of the die is kept extremely close to the value imposed by the TEC.

B. IMPACT OF THE CARRIER ON THE LED CHARACTERISTICS

T_J impacts directly the LED characteristics such as emission intensity, lifetime, and wavelength stability. The variation of each parameter with T_J is analyzed in detail in the following paragraphs. To facilitate the interpretation of the results, the impact of the carrier on the emission intensity and lifetime is evaluated considering the emission intensity and lifetime obtained with AlN and $\kappa = 193$ W/(m·K) as a reference.

Similarly to other p-n junctions, the current that flows through an LED increases with increasing temperature due (among other factors) to the dependency of the carrier concentration on the temperature given by the Boltzmann equations

$$n = N_C \cdot \exp\left(-\frac{E_C - E_F}{k_B \cdot T}\right) \quad (1)$$

and

$$p = N_V \cdot \exp\left(\frac{E_V - E_F}{k_B \cdot T}\right) \quad (2)$$

for electrons and holes, respectively. In these equations, N_C and N_V are the effective densities of states in the conduction and valence bands in the n and p sides of the junction, respectively, E_C and E_V are the bottom and top of the conduction and valence bands, respectively, E_F is the Fermi level, k_B is the Boltzmann constant, and T is the junction temperature. However, in the case of LEDs, the temperature-induced increase of the current does not translate to an increased emission intensity because, as temperature rises, non-radiant recombination (such as Shockley Read Hall and Auger recombination) increases, whereas radiative recombination (the source of the LED light emission) decreases. Carrier loss over the heterostructure barriers, which contributes to the decrease of the LED emission efficiency, also increases with temperature. For more details on the related physical phenomena the readers are referred to works such as [2].

Near room temperature the dependence of the emission intensity on the temperature may be described by the phenomenological equation:

$$I = I_{300K} \cdot \exp\left(-\frac{T - 300}{T_1}\right), \quad (3)$$

where I_{300K} is the emission intensity at 300 K and T_1 is the characteristic temperature, an empirical parameter that depends on the heterojunction layers of a particular device [2]. In the current case, however, this equation was of no use since the manufacturer does not give details about the structure of the active layers of the LED - which prevents the determination of the characteristic temperature. Instead, the impact of the carrier material on the emission intensity was estimated using the characteristic curves representing the RLF as a function of T_J provided by the manufacturer for a current of 350 mA [27] (Fig. 5(a)). The dependence of T_J on I was considered independent of the LED color; under this assumption, the values of T_J obtained with each carrier at 350 mA can be used to estimate the value of the RLF for each type of LED using the respective curve in Fig. 5(a). The ratio between the RLF obtained at 350 mA with each carrier and the RLF obtained with an AlN carrier ($\kappa = 193$ W/(m·K)) is represented in Fig. 5(b) for the blue, green, amber, and red LEDs. The green LED does not show a measurable variation of the RLF with the carrier, whereas the RLF of the amber LED increases (or decreases) by 2% (by 10%) when AlN is replaced with diamond 2200 W/(m·K) (Al_2O_3, 27 W/(m·K)).

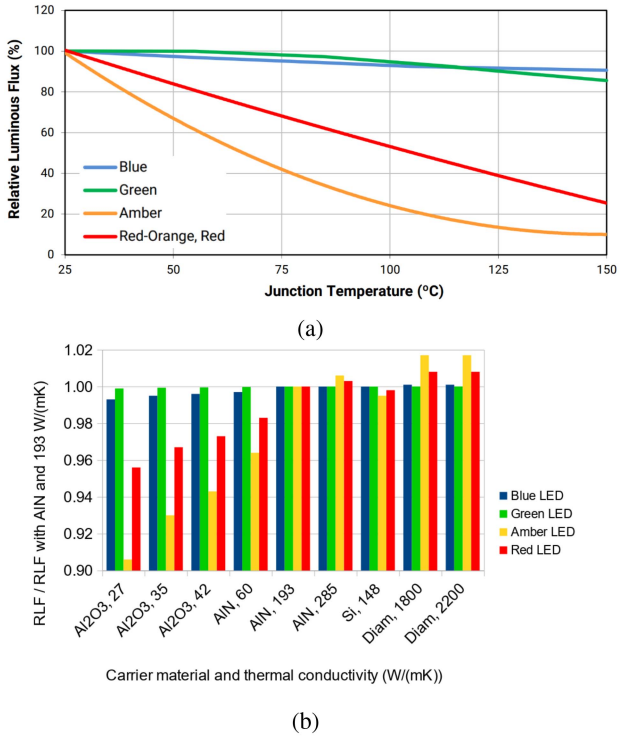

FIGURE 5. (a) RLF as a function of T_J for 350 mA. Image obtained from the device datasheet [27]. (b) Relative variation of RLF with respect to the values obtained with AlN (κ = 193 W/(m·K)).

The carrier also influences the lifetime directly. It is generally accepted by the semiconductor industry to determine the Time-to-Failure (TTF) of a device using the Black model [46], [47]:

$$TTF = I_0 \cdot J^{-n} \cdot \exp\left(\frac{q \cdot E_a}{k_B \cdot T}\right), \tag{4}$$

where I_0 is a constant, J is the current density, n is a scaling factor, q is the electron charge, E_a is the activation energy of the failure mechanisms (in eV), k_B is the Boltzmann constant, and T is the junction temperature (in K). As expected, the TTF decreases as the junction temperature increases. Typically manufacturers do not provide the numerical values of the constants I_0, n, and E_a, so the lifetime of the device cannot be calculated directly. Instead, it is common to consider the lifetime under nominal operating conditions, and to evaluate the impact of elevated operating temperatures on the lifetime by calculating the so-called acceleration factor (AF). The AF based on the Black model can be defined as:

$$AF = \frac{TTF_{nom}}{TTF_{st}} = \left(\frac{J_{st}}{J_{nom}}\right)^n \cdot e^{\frac{q \cdot E_a}{k_B} \cdot \left(\frac{1}{T_{nom}} - \frac{1}{T_{st}}\right)}, \tag{5}$$

where J_{nom} (T_{nom}) and J_{st} (T_{st}) are the current density levels (junction temperature) at the nominal and stress conditions, respectively, and E_A is the activation energy of the failure mechanisms of the semiconductor material. Defined this way, the AF correlates the actual high temperature operating life (HTOL) stress test data points, taken at elevated temperatures and/or current levels, to the expected lifetime under the actual operating conditions in a given application.

In the current case, we can use the AF to estimate the increase/decrease in the lifetime when a given carrier is replaced with another one with higher/lower κ. For a given I, if one considers T_J obtained with AlN (κ = 193 W/(m·K)) as a reference, the AF can be defined as:

$$AF_{AlN193} = \frac{TTF_{AlN193}}{TTF_{car}} = e^{\frac{q \cdot E_a}{k_B} \cdot \left(\frac{1}{T_{J,AlN193}} - \frac{1}{T_{J,car}}\right)}, \tag{6}$$

where $T_{J,AlN193}$ is the junction temperature with the AlN (193 W/(m·K)) carrier and $T_{J,car}$ is the junction temperature obtained with the other carriers. The values of E_A reported in the literature for GaN devices range between 1.05 and 2.5 eV, reflecting the differences in the processes and materials used by the different laboratories and companies around the world [47]. In the lack of data relative to the Cree LEDs, the AF was calculated for the minimum and maximum values of activation energy found in the literature and for two levels of current, 350 mA and 800 mA. The results are presented in Fig. 6. The impact of the carrier on the lifetime is more evident for higher activation energies (Fig. 6(a), logarithmic Y scale). For 350 mA, replacing the AlN (193 W/(m·K)) with the lowest conductivity Al_2O_3 carrier will accelerate the aging of the LED by about 6 times. For the same current, replacing the AlN with the diamond carriers reduces the aging of the LED by $\simeq$25%. If operated at 800 mA the difference becomes more evident: the LED ages 60 times faster with Al_2O_3 and two times slower with diamond. This means that when operated at the higher current level, the lifetime of a GaN LED with 2.5 eV activation energy mounted on a diamond carrier will double relatively to an LED mounted with an AlN (193 W/(m·K)) carrier. Again no significant difference is observed between the performance of SCD and PCD diamond carriers. On the other hand, the crystalline form of AlN increases the lifetime of the LED die by 10% (350 mA) and $\simeq$20% (800 mA) with respect to the ceramic AlN with κ = 193 W/m·K. For an activation energy of 1.05 eV, the impact of the holders is not as large (Fig. 6(b), linear scale). The lowest κ Al_2O_3 carrier accelerates the aging of the LED by a factor of $\simeq$2 and $\simeq$6 for 350 and 800 mA, respectively, while the diamond carrier slows down the aging of the LED by $\simeq$10% and $\simeq$30% at the same current levels.

The final parameter that is directly influenced by T_J is the wavelength of the emitted radiation, λ. When the thermal energy of the charge carriers $k_B \cdot T$ (k_B being the Boltzmann constant and T the temperature) is small compared to the bandgap energy E_g, the frequency of the emitted photons (ν) is given by:

$$\nu = E_g/h, \tag{7}$$

where h is the Planck's constant. On the other hand, the wavelength of the emitted photons can be calculated as $\lambda = c/\nu$, where c is the velocity of light. Combining this with

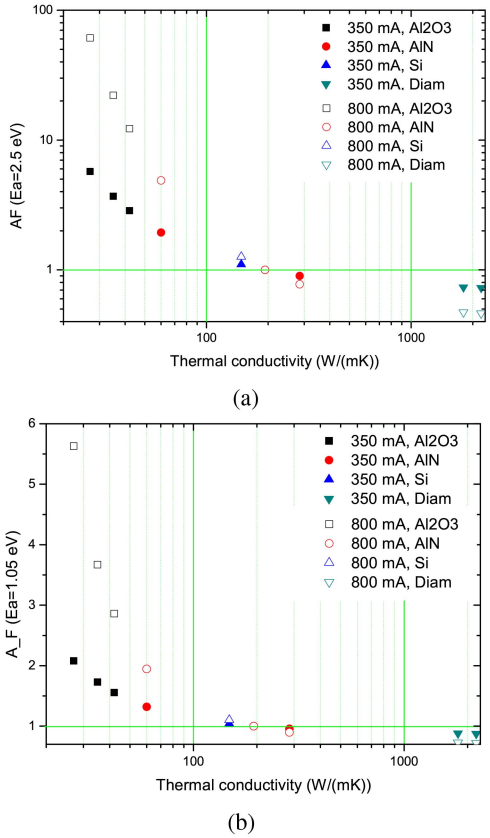

FIGURE 6. **Acceleration factor induced by replacing the AlN (193 W/(m·K)) carrier with the other carriers for current levels of 350 and 800 mA. (a) $E_A = 2.5$ eV activation energy (logarithmic Y scale). (b) $E_A = 1.05$ eV (linear Y scale).**

Eq. (7) gives the following expression:

$$\lambda = \frac{c \cdot h}{E_g}. \tag{8}$$

The temperature dependence of the bandgap energy E_g is commonly expressed by the empirical Varshni equation [48]:

$$E_g(T) = E_g(0) - \frac{\alpha \cdot T^2}{T + \beta}, \tag{9}$$

where $E_g(0)$ is the bandgap energy at a temperature of 0 K, T is the temperature, and α and β are empirical parameters characterizing the particular semiconductor material.

To estimate the dependency of the wavelength of the blue, green, and red Cree LEDs on the carrier material, the wavelength at 300 K was initially determined from the device datasheet. The bandgap energy at 300 K ($E_g(300)$) was calculated by replacing the wavelength in Eq. (8). Considering $\alpha = 9.4 \times 10^{-4}$ eV/K and $\beta = 791$ K [49] and replacing $E_g(300)$ in Eq. (9), $E_g(0)$ was finally determined. The calculated values are listed in Table 2.

Following the extraction of these parameters, the values of E_g for the blue, green, and red LEDs and the different carriers/current levels were calculated by replacing the simulated values of T_J in Eq. (9). Finally, the values of $E_g(T)$ were replaced in Eq. (8), allowing the determination of λ for all the carriers and current values. It was seen that λ increases linearly with I. The slope of each $\lambda(I)$ curve was determined from the graphs in the current range 100-800 mA and the results are plotted in Fig. 7. For each carrier, the drift of λ with I is larger for the red LED and smaller for the blue LED. These results are a consequence of the larger bandgap of blue LEDs (2.51 eV) in comparison to the red LEDs (1.85 eV). The drift of λ decreases with the increase in the κ of the carrier: the maximum values of ≃3.8/2.1 nm/A for the red/blue LEDs are obtained with the Al_2O_3 (27 W/(m·K)). When the same LED dies are mounted on the diamond carriers, the λ drift decreases to ≃ 0.2 and 0.1 nm/A for the red and blue LEDs, respectively.

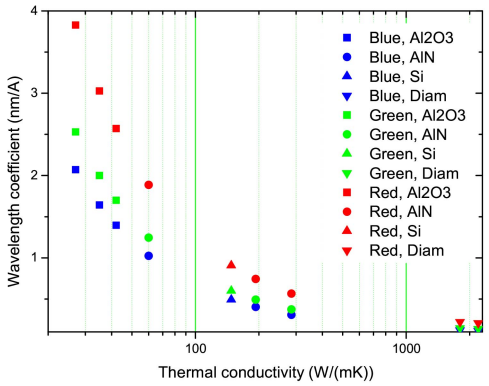

FIGURE 7. **Coefficient of variation of λ with *I*.**

TABLE 2. **Wavelength and bandgap energy for blue, green and red Cree LEDs.**

LED	$\lambda(300K)$ nm	$E_g(300K)$ eV	$E_g(0K)$ eV
Blue	467	2.51	2.59
Green	515	2.28	2.35
Red	633	1.85	1.93

C. ADVANTAGES OF DIAMOND CARRIERS

As expected, all the LEDs characteristics improve when materials with higher κ are used as die carriers and the choice of a given material over the others should be made taking into consideration the required performance of the LED. Lower cost Al_2O_3 and AlN ceramic holders with different κ are available from a variety of manufacturers. Diamond holders can be purchased from a few vendors and are available in two forms. SCD plates with κ as high as 2200 W/(m·K) are manufactured by high power high temperature (HPHT) method [13]; this material shows the lowest concentration of defects and, consequently, the best properties. However, the area of SCD crystals is limited to a few mm^2. On the other hand, larger area PCD wafers deposited by chemical vapour deposition (CVD) show a larger number of defects, nevertheless κ remains as high as 1800 W/(m·K). Curiously,

the simulations showed that the performance of the LED dice mounted SCD of PCD carriers is similar.

The replacement of the currently used AlN carrier with a diamond one would improve the reliability of power LEDs at different levels. In terms of the light intensity, for nominal current level the impact of the carrier is minimal. The amber LED shows the largest change in the light intensity. When compared to the RLF of a LED mounted on an AlN carrier with $\kappa = 193$ W/(m·K), replacing it with an AlN carrier with 60 W/(m·K) or a diamond carrier results in $\simeq$96.4% and $\simeq$101.7% of the initial intensity of light. It can thus be concluded that at nominal current levels the κ of the carrier has a minor impact on the intensity of the emission.

The impact of the carrier on the lifetime is quite relevant. For nominal current level and considering the 193 W/(m·K) AlN carrier as a reference, replacing it with diamond increases the lifetime to 10% (350 mA) and 25% (800 mA) for the lowest activation energy, and to 30% (350 mA) and 50% (800 mA) for the highest activation energy.

The diamond carriers also improve the stability of the λ of the emitted light with the temperature; the drift of the λ is as low as 0.2 nm/A for the red LED and 0.1 nm/A for the blue and green LEDs. With the AlN (193 W/(m·K)) carrier, the drift increases to 0.7, 0.5 and 0.4 nm/A for the same LEDs, respectively.

Finally, the use of diamond carriers minimizes the LED footprint. The temperature at the edge of the AlN (193 W/(m·K)) carrier is 40.23 and 40.58°C for 350 and 800 mA, respectively (Fig. 2(c)). On the other hand, the temperature at the edge of the diamond carrier remains as low as 40.2° C for 800 mA (Fig. 2(c)). Looking at Fig. 4(b) it becomes clear that, even for high current levels, the footprint of the die is considerably smaller than that of the carrier, allowing the use of smaller carriers and the increase of the total power density.

Due to the positive impact of the diamond carrier on the characteristics of power LEDs, it can be said that CVD diamond would be the material of choice for high power applications. However, due to the high cost of the plates (around 300€/cm^2 for individual plates), their effective use is only an option for very demanding applications, such as the space industry, where reliability and lifetime are critical factors. As an example, let us consider the Lisa (Laser Interferometer Space Antenna) Pathfinder ESA mission, that intends to test in flight the concept of gravitational wave detection by putting two test masses in a near-perfect gravitational free-fall and controlling and measuring their motion with unprecedented accuracy [50]. LISA Pathfinder discharge system currently exploits the photoelectric effect using UV radiation emitted by mercury (Hg) lamps following the method demonstrated by Gravity Probe B [51]. Since the development of this mission, UV LEDs have become commercially available from different manufacturers. These LEDs offer many advantages over traditional Hg lamps, such as a lower mass and volume, increased electrical efficiency, faster response times and the possibility of using light of a shorter wavelength [52]. Even though the results reported in this paper were obtained with Cree white and different colored power LEDs, the results can be directly extrapolated for UV LEDs. The heat management of UV LED dies would be dramatically improved by mounting the LED die directly on a diamond carrier, with a positive impact on the lifetime, on the overall emission efficiency, on the stability of the emitted UV radiation, and on the footprint of the devices. Altogether this means that with the diamond carrier the current levels that can be injected in the LEDs without compromising the lifetime would be maximized, and, at the same time, the footprint of the LED (and the corresponding volume and weight) would be decreased.

Despite the unquestionable benefits of diamond plates, there are still some open questions that require further research. To the authors' best knowledge, assembling a die with a diamond carrier would not be any different than assembling it with, for instance, an AlN carrier. The die and the carrier are "glued" together using a layer of die attach material. Depending on the required properties of the die attach (namely thermal and electrical conductivities), this material can be an epoxy, solder paste, or a eutectic alloy (among others). The reliability of the power LED will ultimately depend on the robustness of this die attach layer – which will have to keep the mechanical bond between the die and the carrier during device operation. However, due to the different coefficients of thermal expansion (CTEs) of the LED die (3.06×10^{-6} K^{-1} in the case of single crystal SiC substrate [53]) and the carrier (1, 5.6, and 8×10^{-6} K^{-1} for diamond [39], ceramic AlN [34], and ceramic Al_2O_3 [32], respectively), the die attach will suffer from thermal cycling effects as the LED is switched on and off. The thermal stress that will have to be accommodated by the die attach depends on the difference between the CTEs of the different materials and on the temperature gradient between the bottom of the SiC substrate and the top of the carrier. The difference in the CTEs is maximal for the diamond plate but simultaneously the temperature gradient is minimal, so it is not possible to predict the thermal cycling effects with the diamond carrier without a thorough study. The low standard roughness of a diamond plate, as provided by the manufacturer (< 10 nm) may, in itself, present an additional problem, since it may hamper the mechanical interlock between the die attach and the diamond carrier. These topics will be a part of our future research. As a last comment, for simplicity, the thickness of the different carriers was considered to be 540 μm. Since the cost of diamond plates increases with the thickness, in a real application the diamond carrier should be as thin as possible – while still being mechanically robust not to break during assemblage with the LED die. The thickness suggested by the manufacturers is 300 μm. Thicker plates, available at a higher cost, would provide marginal benefits.

IV. CONCLUSION

The impact of the thermal conductivity of the GaN-SiC die carrier on the lifetime, relative luminous flux and wavelength stability of a Cree power LED was evaluated through thermal simulations performed with Ansys. Different materials were considered, such as ceramic and single crystalline Al_2O_3 and AlN, crystalline Si, SCD, and PCD. The difference in the junction temperature obtained with Al_2O_3 (27 W/(m·K)) and SCD (2200 W/(m·K)) is 7.2° C and 17.6° C for a current level of 350 and 800 mA, respectively. The coefficient of variation of the junction temperature with the current for both materials is 24 and 1.4° C/A, respectively. For nominal current levels, the dependence of the RLF of blue and green LEDs on the carrier material is not relevant, unlike the amber LED that shows a decrease of 10% and an increase of 2% when an AlN carrier (193 W/(m·K)) is replaced with Al_2O_3 (27 W/(m·K)) and diamond (2200 W/(m·K)), respectively. The lifetime of the LEDs varies considerably with the carrier material. Using the lifetime of the LED mounted on the AlN (193 W/(m·K)) carrier as a reference and an activation energy of 2.5 eV, the AF increases with the Al_2O_3 (27 W/(m·K)) holder by almost 6 times and by more than 60 times for a current level of 350 and 800 mA, respectively, whereas for the same current levels it decreases to 0.75 and less than 0.5 with the diamond (2200 W/(m·K)) carrier. Finally, the impact of both materials on the drift of the wavelength with the current level was also evaluated, being minimal for the blue LEDs and maximal for the red LEDs. For the later LEDs the drift was 3.8 and 0.2 nm/A with Al_2O_3 (27 W/(m·K)) and diamond (2200 W/(m·K)), respectively. The quality of Al_2O_3 and AlN carriers has a considerable impact on all the figures, unlike what happens with both SCD and PCD carriers, that have comparable thermal performance. Given the tremendous impact of the carrier material on the junction temperature, and consequently, on all the LED figures, the choice of the carrier material is highly dependent on the required performance of the LED. For applications such as the gravitational wave detection, the use of PCD carriers may increase the lifetime and improve the performance of the UV LED light sources, which are critical for the success of the mission.

ACKNOWLEDGMENT

The authors would like to thank Cree for providing information regarding the structure of the LED and ANSYS support team for providing technical support during the simulations. Dr. Joana C. Mendes was hired by Instituto de Telecomunicações under the decree law Nr. 57/2016.

REFERENCES

[1] P. Liu *et al.*, "Thermal simulations of a UV LED module with nanosilver sintered die attach process on graphene-coated copper substrates," in *Proc. 16th China Int. Forum Solid-State Light. Int. Forum Wide Bandgap Semicond. China (SSLChina: IFWS)*, 2019, pp. 93–97.

[2] E. F. Schubert, *Light-Emitting Diodes*. Cambridge, U.K.: Cambridge Univ. Press, 2006.

[3] R. H. Horng *et al.*, "Thermal management design from chip to package for high power InGaN/Sapphire LED applications," *Electrochem. Solid-State Lett.*, vol. 12, no. 6, p. H222, 2009.

[4] R. Liang *et al.*, "Investigation on thermal characterization of eutectic flip-chip UV-LEDs with different bonding voidage," *IEEE Trans. Electron Devices*, vol. 64, no. 3, pp. 1174–1179, Mar. 2017.

[5] M. Y. Tsai, C. Y. Tang, C. Y. Yen, and L. B. Chang, "Bump and underfill effects on thermal behaviors of flip-chip LED packages: Measurement and modeling," *IEEE Trans. Device Mater. Rel.*, vol. 14, no. 1, pp. 161–168, Mar. 2014.

[6] M. Shatalov *et al.*, "Thermal analysis of flip-chip packaged 280 nm nitride-based deep ultraviolet light-emitting diodes," *Appl. Phys. Lett.*, vol. 86, no. 20, pp. 1–3, 2005.

[7] C. Y. Tang, M. Y. Tsai, C. C. Lin, and L. B. Chang, "Thermal measurements and analysis of flip-chip led packages with and without underfills," in *Proc. Int. Microsyst. Packag. Assembly Circuits Technol. Conf. IMPACT Int. 3-D IC Conf.*, May 2018, pp. 2–6.

[8] K. L. Chun, M. J. Dai, C. K. Yu, and S. L. Kuo, "High efficiency silicon-based high power LED package integrated with micro- thermoelectric device," in *Proc. Techn. Papers Int. Microsyst. Packag. Assembly Circuits Technol. Conf. (IMPACT)*, 2007, pp. 29–33.

[9] B. Fan, H. Wu, Y. Zhao, Y. Xian, B. Zhang, and G. Wang, "Thermal study of high-power nitride-based flip-chip light-emitting diodes," *IEEE Trans. Electron Devices*, vol. 55, no. 12, pp. 3375–3382, Dec. 2008.

[10] A. A. Balandin, "Thermal properties of graphene and nanostructured carbon materials," *Nat. Mater.*, vol. 10, no. 8, pp. 569–581, 2011. [Online]. Available: http://dx.doi.org/10.1038/nmat3064

[11] E. Pop, V. Varshney, and A. K. Roy, "Thermal properties of graphene: Fundamentals and applications," *MRS Bull.*, vol. 37, no. 12, pp. 1273–1281, 2012.

[12] P. Huang *et al.*, "Graphene film for thermal management: A review," *Nano Mater. Sci.*, vol. 3, no. 1, pp. 1–16, 2021. [Online]. Available: https://doi.org/10.1016/j.nanoms.2020.09.001

[13] J. J. Gracio, Q. H. Fan, and J. C. Madaleno, "Diamond growth by chemical vapour deposition," *J. Phys. D Appl. Phys.*, vol. 43, no. 37, pp. 1–22, 2010.

[14] C. B. Swan, "Improved performance of silicon avalanche oscillators mounted on diamond heat sinks," *Proc. IEEE*, vol. 55, no. 9, pp. 1617–1618, Sep. 1967.

[15] J. V. D. S. Neto, M. A. Fraga, and V. J. Trava-Airoldi, "Development, properties, and applications of CVD diamond-based heat sinks," in *Some Aspects of Diamonds in Scientific Research and High Technology*, E. Lipatov, Ed. London, U.K.: IntechOpen, 2020, ch. 4, pp. 1–18. [Online]. Available: https://www.intechopen.com/books/some-aspects-of-diamonds-in-scientific-research-and-high-technology/development-properties-and-applications-of-cvd-diamond-based-heat-sinks

[16] A. J. Kemp *et al.*, "Thermal management of lasers and leds using diamond," *Opt. Eng. Diamond*, pp. 353–384, Mar. 2013.

[17] S. Z. Rotter and S. L. Heidger, "Integrated diamond carrier for laser bar arrays," 2009.

[18] N. V. Apollo *et al.*, "Cooling of miniature electronic systems using diamond circuit boards," in *Proc. 17th InterSoc. Conf. Thermal Thermomech. Phenom. Electron. Syst. (ITherm)*, 2018, pp. 340–344.

[19] X. Jia *et al.*, "The influence of dielectric layer on the thermal boundary resistance of GaN-on-diamond substrate," *Surface Interface Anal.*, vol. 51, no. 7, pp. 783–790, 2019.

[20] Z. Cheng, F. Mu, L. Yates, T. Suga, and S. Graham, "Interfacial thermal conductance across room-temperature bonded GaN-diamond interfaces for GaN-on-diamond devices," *ACS Appl. Mater. Interfaces*, vol. 12, no. 7, pp. 8376–8384, Jan. 2020.

[21] R. Ahmed, A. Siddique, J. Anderson, C. Gautam, M. Holtz, and E. Piner, "Integration of GaN and diamond using epitaxial lateral overgrowth," *ACS Appl. Mater. Interfaces*, vol. 12, no. 35, pp. 39397–39404, 2020.

[22] M. D. Smith *et al.*, "GaN-on-diamond technology platform: Bonding-free membrane manufacturing process," *AIP Adv.*, vol. 10, no. 3, pp. 1–6, 2020. [Online]. Available: https://doi.org/10.1063/1.5129229

[23] A. E. Helou *et al.*, "High-resolution thermoreflectance imaging investigation of self-heating in AlGaN/GaN HEMTs on Si, SiC, and diamond substrates," *IEEE Trans. Electron Devices*, vol. 67, no. 12, pp. 5415–5420, Dec. 2020.

[24] P. H. Chen, C. L. Lin, Y. K. Liu, T. Y. Chung, and C. Y. Liu, "Diamond heat spreader layer for high-power thin-GaN light-emitting diodes," *IEEE Photon. Technol. Lett.*, vol. 20, no. 10, pp. 845–847, May 2008.
[25] Y. Fan *et al.*, "Pressure infiltrated Cu/diamond composites for LED applications," *Rare Metals*, vol. 30, no. 2, pp. 206–210, 2011.
[26] R. Xie, Z. Li, S. Guo, Z. Wang, and H. Xue, "High bandwidth GaN-based blue LEDs using Ag-grating and diamond heat sink," *Photon. Nanostruct. Fundam. Appl.*, vol. 42, Dec. 2020, Art. no. 100856. [Online]. Available: https://doi.org/10.1016/j.photonics.2020.100856
[27] Cree. (2015). *Cree XLamp XB-D LEDs Datasheet*. [Online]. Available: https://www.cree.com/led-components/media/documents/ds-XBD.pdf
[28] Cree. (2018). *Cree XLamp LED Long-Term Lumen Maintenance Application Note*. [Online]. Available: https://www.cree.com/led-components/media/documents/XLamp_lumen_maintenance.pdf
[29] Digi-Key. (2015). *Silicon Carbide Substrate Boosts LED Luminosity*. [Online]. Available: https://www.digikey.com/en/articles/silicon-carbide-substrate-boosts-LED-luminosity
[30] Digi-Key. (2013). *Will Silicon Substrates Push LED Lighting Into the Mainstream?* [Online]. Available: https://www.digikey.com/en/articles/will-silicon-substrates-push-led-lighting-into-the-mainstream
[31] S. Liu and X. Luo, *LED Packaging for Lighting Applications: Design, Manufacturing and Testing*. Hoboken, NJ, USA: Wiley, 2011.
[32] P. J. Karditsas and M.-J. Baptiste. *Thermal and Structural Properties of Fusion Related Materials*. [Online]. Available: http://aries.ucsd.edu/LIB/PROPS/PANOS/
[33] Kyocera. (2020). *Single Crystal Sapphire*. [Online]. Available: https://global.kyocera.com/prdct/fc/product/pdf/s_c_sapphire.pdf
[34] Azo Materials. (2001). *Aluminium Nitride—Properties and Applications*. [Online]. Available: https://www.azom.com/properties.aspx?ArticleID=610
[35] D. Huang, Z. Liu, J. Harris, X. Diao, and G. Liu, "High thermal conductive AlN substrate for heat dissipation in high-power LEDs," *Ceramics Int.*, vol. 45, no. 1, pp. 1412–1415, 2019. [Online]. Available: https://doi.org/10.1016/j.ceramint.2018.09.171
[36] G. A. Slack, R. A. Tanzilli, R. O. Pohl, and J. W. Vandersande, "The intrinsic thermal conductivity of AIN," *J. Phys. Chem. Solids*, vol. 48, no. 7, pp. 641–647, 1987.
[37] EL-CAT Inc. *Properties of Silicon*. [Online]. Available: https://www.el-cat.com/silicon-properties.htm
[38] Diamond Materials. *Thermal Properties of CVD Diamond*. [Online]. Available: https://www.diamond-materials.com/en/cvd-diamond/thermal/
[39] Diamond Materials. (2014). *The CVD Diamond Booklet*. [Online]. Available: http://www.diamond-materials.com/downloads/cvd_diamond_booklet.pdf
[40] C. Mion, J. F. Muth, E. A. Preble, and D. Hanser, "Accurate dependence of gallium nitride thermal conductivity on dislocation density," *Appl. Phys. Lett.*, vol. 89, no. 9, pp. 1–3, 2006.
[41] Wolfspeed. (2020). *GaN on SiC: The Substrate Challenge*. [Online]. Available: https://www.wolfspeed.com/knowledge-center/article/gan-on-sic-the-substrate-challenge
[42] Engineers Edge. *Thermal Properties of Metals, Conductivity, Thermal Expansion, Specific Heat*. [Online]. Available: https://www.engineersedge.com/properties_of_metals.htm
[43] M. Y. Tsai, C. H. Chen, and C. S. Kang, "Thermal measurements and analyses of low-cost high-power LED packages and their modules," *Microelectron. Rel.*, vol. 52, no. 5, pp. 845–854, 2012, doi: 10.1016/j.microrel.2011.04.008.
[44] Cree. (2015). *Thermal Management of Cree XLamp Application Note*. [Online]. Available: https://www.cree.com/led-components/media/documents/XLampThermalManagement.pdf
[45] Cree. (2021). *Cree XLamp-XBD Spice Model*. [Online]. Available: https://cree-led.com/media/documents/XLamp-XBD-Spice.txt
[46] J. R. Black, "Electromigration—A brief survey and some recent results," *IEEE Trans. Electron Devices*, vol. ED-16, no. 4, pp. 338–347, Apr. 1969.
[47] S. R. Bahl, *A Comprehensive Methodology to Qualify the Reliability of GaN Products*, Texas Instrum., Dallas, TX, USA, 2015. [Online]. Available: http://www.ti.com/lit/wp/slyy070/slyy070.pdf
[48] Y. P. Varshni, "Temperature dependence of the energy gap in semiconductors," *Physica*, vol. 34, no. 1, pp. 149–154, 1967.
[49] N. Nepal, J. Li, M. L. Nakarmi, J. Y. Lin, and H. X. Jiang, "Temperature and compositional dependence of the energy band gap of AlGaN alloys," *Appl. Phys. Lett.*, vol. 87, no. 24, 2005, Art. no. 242104.
[50] ESA. *LISA Pathfinder*. [Online]. Available: https://sci.esa.int/web/lisa-pathfinder
[51] S. Buchman *et al.*, "The gravity probe B relativity mission," *Adv. Space Res.*, vol. 25, no. 6, pp. 1177–1180, 2000.
[52] D. Hollington, J. T. Baird, T. J. Sumner, and P. J. Wass, "Lifetime testing UV LEDs for use in the LISA charge management system," *Classical Quant. Gravity*, vol. 34, no. 20, pp. 1–15, 2017.
[53] M. Stockmeier, R. Müller, S. A. Sakwe, P. J. Wellmann, and A. Magerl, "On the lattice parameters of silicon carbide," *J. Appl. Phys.*, vol. 105, no. 3, pp. 1–4, 2009.